Influence of Gd$_2$O$_3$ reinforcement on the mechanical, physical and radiation shielding properties of Al-30Sm$_2$O$_3$ composites

Seyit Çağlar[1]

Abstract - In this comprehensive study, we meticulously fabricated Al-30Sm$_2$O$_3$-XGd$_2$O$_3$ (X = 3, 6, 9, 12, and 15) composites through a series of tests and analyses to determine the composites' mechanical, physical, corrosion, and radiation shielding properties. Scanning electron microscopy (SEM-EDX) and X-ray diffraction (XRD) techniques were used for microstructural analysis. The main objective of the research is to investigate the effects of Gd$_2$O$_3$ reinforcement on the mechanical properties (hardness, wear resistance, and corrosion resistance) and radiation shielding performances of the composites. MCNP6.2 simulations evaluated thermal, fast neutron, and gamma-ray attenuation properties, while mechanical properties were analyzed by hardness, wear, and corrosion tests. XRD analyses showed no intermetallic phase was formed, while SEM-EDX analyses revealed that the composites were homogeneous and had a partial increase in void ratio with Gd$_2$O$_3$ reinforcement. Gd$_2$O$_3$ reinforcement increased the hardness and wear resistance of the composites, but a slight decrease in relative density was observed. The highest hardness and wear resistance were obtained at 15% Gd$_2$O$_3$ reinforcement. The corrosion rate decreased with Gd$_2$O$_3$ reinforcement, while an increase in corrosion rate was observed in the composite containing 15% Gd$_2$O$_3$. MCNP6.2 simulations showed that Gd$_2$O$_3$ reinforcement increased the thermal neutron macroscopic cross-section and linear attenuation coefficient while decreasing the fast neutron macroscopic cross-section.

1. Introduction

Nuclear technology is used in many areas of our lives, such as medical, industrial, research, education, security applications, and consumer products. Nevertheless, nuclear radiation is also produced during the use of nuclear technology, and this can be extremely dangerous for public safety, the environment, and human health. Moreover, radiation can cause serious health problems such as nerve damage, reproductive issues, heart disease, and cancer, in addition to its benefits due to its uses [1,2]. For this reason, radiation metal matrix composite, polymer, and glass shielding materials are being developed according to the needs of the radiation-emitting area to protect personnel working in areas where radiation is used/emitted [3–6].

Boron carbide (B$_4$C) reinforced Aluminum matrix composites (AMCs) have been studied due to the high thermal neutron absorption cross-section of boron. However, augmenting the B$_4$C content in Al-B$_4$C composites limits the thermal neutron macroscopic absorption rate by diminishing machinability and corrosion resistance [7–13]. This situation limits the B$_4$C content and the thermal neutron cross-section in Al-B$_4$C composites. [14–17]. However, rare earth elements are expensive and have a high tendency to oxidize, making them challenging to study and produce, so research is turning to using oxides of rare earth elements. Using Sm$_2$O$_3$ and Gd$_2$O$_3$ ceramics as reinforcing elements provides advantages in terms of increasing mechanical properties and cost.

[1]caglar.s@yandex.com, s.caglar@beun.edu.tr (Corresponding Author)
[1]Department of Metallurgical and Materials Engineering, Zonguldak Bülent Ecevit University, Zonguldak, Türkiye

World reserves of samarium are known to be around 2 million tons. In addition, samarium is found and processed in many countries, such as China, the USA, India, Brazil, Sri Lanka, and Australia [18,19]. The fact that an element has different logistics networks is critical for industrial use. This situation is called a perfect competition market in economics, the fairest market. As a result, problems such as price fluctuations and supply problems are eliminated. This makes Sm_2O_3 a suitable reinforcement element in terms of cost-effectiveness. Furthermore, it has a neutron cross-section compared to elemental neutron shielding, such as samarium, boron, and cadmium.

Al6061 has been and continues to be used in many areas worldwide for its low density, high reserves, easy procurement process, corrosion resistance, machinability, and good wear properties. Furthermore, Al6061 is a matrix material to prepare AMCs due to its exceptional formability [20–22]. Among the elements such as Eu, Sm, B, Dy, Tb, and Gd used as reinforcements, Gd has the highest thermal neutron attenuation cross-section and stands out with its gamma-ray attenuation capability (LAC). Due to the superior properties of Gd and Gd_2O_3 doped composites, it is considered an alternative MMC to the existing and frequently studied Al-B_4C composites in the literature. When small amounts of Gd are added to the 30% Al-B_4C composition, which is accepted as an ideal ratio in the literature, instead of B_4C, it is observed that the obtained Al-B_4C-Gd composite increases the thermal neutron cross-section while improving mechanical properties such as toughness, machinability, and elongation amount [23]. However, gadolinium is a highly reactive element that reacts quickly with oxygen.

For this reason, Gd_2O_3, which emerged as a cheaper alternative to pure Gd, stands out in terms of sustainability. Gd_2O_3 is considered an excellent additive material because it has a high thermal neutron cross-section with low Gadolinium content and is cheaper than B_4C. In the composites, Gd_2O_3 serves as a reinforcement element, enhancing the mechanical and radiation attenuation properties of the Al matrix. Replacing B_4C with Gd_2O_3 and Sm_2O_3 increases tensile stress and thermal efficiency while maintaining tensile strength by reducing the amount of ceramic particles in the composite [24–26].

The primary goal of this research is to introduce a novel approach to reinforcing the Al matrix with Sm_2O_3 and Gd_2O_3. The fabrication of Al6061-30Sm_2O_3-XGd_2O_3 (X = 3, 6, 9, 12, and 15) composites not only provides new avenues for investigating the effects of different Gd_2O_3 ratios on mechanical and physical properties but also holds promise for the development of advanced radiation shielding materials. These findings have the potential to significantly impact the field of materials science, leading to the development of new applications in various sectors.

2. Material and Methods

2.1. Sample Preparation and Characterization

The synthesis of the composites involved a series of meticulous steps, ensuring the highest research standards. First, Al6061 (15-53 µm), Gd_2O_3 (44 µm), and Sm_2O_3 (44 µm) powders, each with a purity of approximately 99.9%, were weighed in the proportions shown in Table 1. These powders were then placed in the hoppers of a shaker mill (Chisun Tech), where they underwent a grinding process for 2 hours. The grinding media, consisting of hardened steel balls with a diameter of 15 mm and a hardened steel bowl with a capacity of 80 ml, were used at 40 Hz. The ball-to-powder weight ratio was kept at 10:1. To ensure accuracy and prevent overheating, a 2-minute pause was set every 5 minutes during the grinding process.

After grinding, the powders were molded into pellets by uniaxial cold pressing at 750 MPa pressure for one minute. The resulting 10 mm diameter pellets were sintered in a Protherm vacuum furnace under an argon atmosphere at 600°C for 2 hours. The relative densities of the sintered samples were determined with a WSA224 density measurement kit using Archimedes' principle.

A Panalytical Empyrean diffractometer and X-ray diffraction (XRD) were used to identify the phases formed by sintering. Surface morphology and elemental distribution were evaluated using an Oxford X-MaxN 80 energy dispersive X-ray spectroscopy (EDX) system and an FEI QUANTA 450 scanning electron microscope (SEM). Vickers microhardness was measured ten times with a Shimadzu HMV-G21 tester using a 100 g load and 15 seconds holding time, and the results were averaged. Wear tests were performed with a total distance of 100 m, a load of 7 N, and a sliding velocity of 12 m/s. Following the abrasion tests, the area of the abrasion marks was measured using a Taylor Hobson 2D profilometer. All abrasion tests were carried out at a constant humidity of 55%-60% and room temperature of 24-29°C using the data obtained from measuring the wear marks using the following formula.

The wear rate was calculated using the data obtained from measuring the wear marks using the following formula

$$WR = \frac{V}{S} \tag{2.1}$$

V: Wear volume (mm³), S: Sliding distance.

Electrochemical tests were conducted at 25 ± 2°C in 3.5% NaCl solution using a Gamry Reference 1010 E electrochemical workstation. Corrosion rates were calculated using equivalent weight for each sample, and theoretical densities were determined using the mixing rule. Furthermore, the synthesis and characterization steps of $Al6061-B_4C-Gd_2O_3$ composites are schematically shown in Figure 2.

The corrosion rate was calculated using the following formula:

$$CR = k\frac{i_{corr}\,EW}{\rho} \tag{2.2}$$

where k= $3.27\text{x}10^3$, constant; I_{corr} = corrosion current density (μA.cm^{-2}); EW = equivalent weight (g.eq^{-1}); and ρ = density (g.cm^{-3}).

2.2. Monte Carlo Simulations

The Monte Carlo N-Particle Program (MCNP) is a versatile and widely used simulation code developed by Los Alamos National Laboratory. It is primarily designed to model the transport and interaction of a wide range of particles, including photons, neutrons, electrons, and other particles such as positrons and heavy ions. The MCNP program uses the Monte Carlo method, a statistical approach that uses random sampling to solve complex problems in nuclear physics, radiation transport, and particle interactions [27]. This study computed gamma-ray linear attenuation coefficient (LAC) and thermal/fast neutron macroscopic cross-sections using the MCNP6.2 code [15,28].

Figure 1 illustrates the intricate simulation geometry, meticulously designed to ensure accurate results. It features a neutron source placed in a cylindrical cavity in a vacuum, a detector (F4 tally) measuring the average flux per cm^2 per source particle, and the target material. The energy of gamma rays is 0.478 MeV (gamma-ray energy from neutron-boron interaction), the energy of thermal neutrons is $2.53*10^{-8}$ MeV, and the fast neutron energy is 2 MeV. Before each simulation, the free flux I_x was calculated without the target material I_0 and with the target material $Al6061-30Sm_2O_3-XGd_2O_3$ (X = 3, 6, 9, 12, and 15). To minimize statistical error, 10^8 neutron histories were generated for each simulation, resulting in a statistical error of less than 1%. (2.3) calculates the gamma-ray, thermal neutron, and fast neutron attenuation ratio. (2.4) and (2.5) were used to calculate the gamma-ray LAC, thermal neutron, and fast neutron macroscopic cross-section using the Beer-Lambert law.

$$\text{\textbf{\textit{Neutron/Gamma Attenuation}} \textbf{Rate}} \ (\%) = \left(1 - \frac{\text{I}_x}{\text{I}_0}\right) \textbf{100} \tag{2.3}$$

$$I_x = I_o e^{-\Sigma_t x} \tag{2.4}$$

$$I_x = I_o e^{-\lambda x} \tag{2.5}$$

where I_o and I_x are the intensities of the incident neutrons-photon and those passing through the absorber, respectively, x is the absorber thickness in centimeters, $\sum_t$ represents the neutron macroscopic cross-section, and λ represents the gamma-ray LAC of the absorber medium.
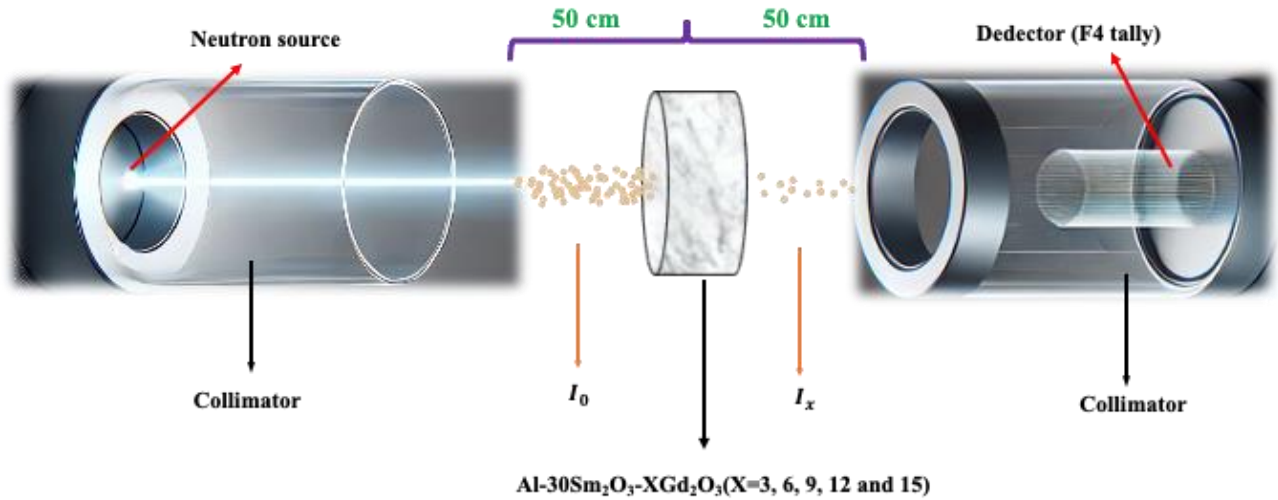
Figure 1. The geometry of the Monte Carlo simulation setup for the Al-Sm_2O_3-Gd_2O_3 composites
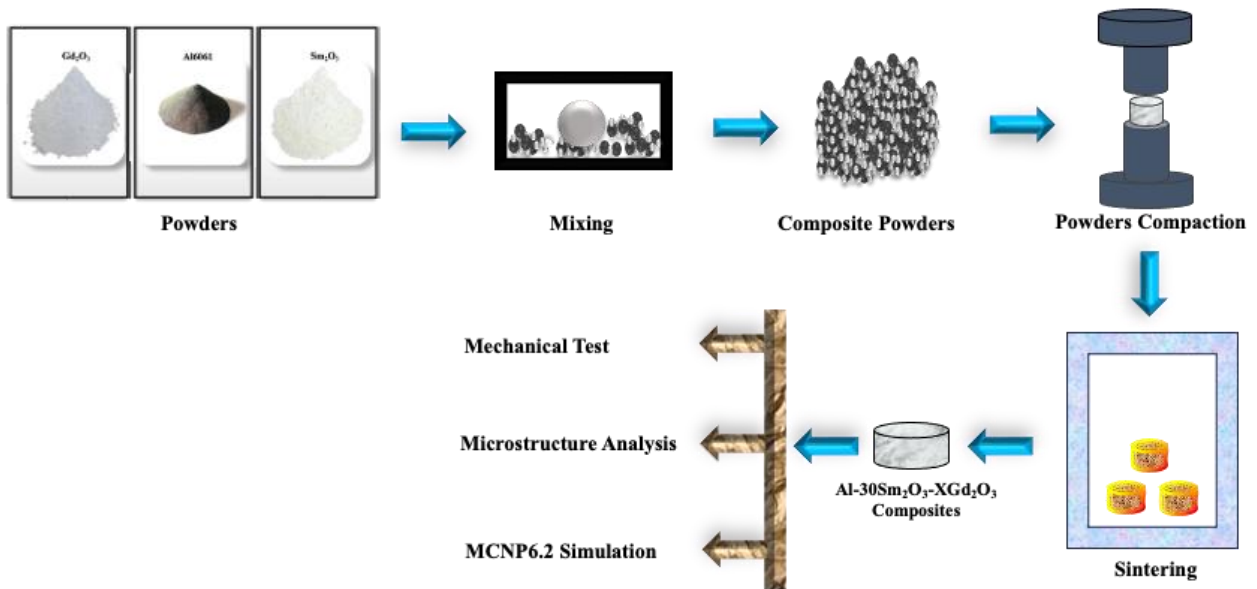
Figure 2. Schematic representation of the Al-Sm_2O_3-Gd_2O_3 composites' production and characterization

3. Results and Discussion

Table 1 displays the weight ratios of the compositions we created for this study, which could be used in various engineering applications. In this comprehensive study, mechanical milling fabricated Al6061-30Sm_2O_3-XGd_2O_3 (X=3, 6, 9, 12, and 15) represented as 3Gd_2O_3, 6Gd_2O_3, 9Gd_2O_3, 12Gd_2O_3, and 15Gd_2O_3 respectively).

Table 1. Chemical compositions of the Al-Sm_2O_3-Gd_2O_3 composites

	Chemical Composition (wt.%)		
	Al	**Sm_2O_3**	**Gd_2O_3**
97(Al-30Sm_2O_3)-3Gd_2O_3	67,9	29,1	3
94(Al-30Sm_2O_3)-6Gd_2O_3	65,8	28,2	6
91(Al-30Sm_2O_3)-9Gd_2O_3	63,7	27,3	9
88(Al-30Sm_2O_3)-12Gd_2O_3	61,6	26,4	12
85(Al-30Sm_2O_3)-15Gd_2O_3	59,5	25,5	15

The density measurements of Al-Sm_2O_3-Gd_2O_3 composites are presented in Table 2. Data analysis reveals that the relative density partially decreases as the Gd_2O_3 content increases in Al-Sm_2O_3-Gd_2O_3 composites, but the measured density values show a corresponding increase. This increase in the experimental results is due to the high density of Gd_2O_3. Although Gd_2O_3 reinforcement is a challenging and difficult-to-compress ceramic, no significant reduction in relative densities occurred. This shows that Gd_2O_3 reinforcement at different ratios into the Al/Sm_2O_3 system is vital for improving composite materials' mechanical and physical properties and neutron and gamma attenuation properties. Especially the absorption of fast neutrons varies proportionally to the relative density; therefore, it is imperative to maintain the relative values.

Table 2. Densities of the Al-Sm_2O_3-Gd_2O_3 composites

	Theoretical Density (g/cm³)	**Experimental Density (g/cm³)**	**Relative Density (%)**
3Gd_2O_3	3,443	3,046	88,457
6Gd_2O_3	3,501	3,075	87,841
9Gd_2O_3	3,561	3,096	86,931
12Gd_2O_3	3,623	3,127	86,300
15Gd_2O_3	3,687	3,178	86,181

3.1. XRD Analysis

The XRD spectra of the Al-Sm_2O_3-Gd_2O_3 composites are depicted in Figure 3. We conducted X-ray diffraction (XRD) analysis to determine the phase distributions and phases in the composites. The study revealed the presence of Al, Sm_2O_3, and Gd_2O_3 phases, confirming the chemical stability of Al-Sm_2O_3-Gd_2O_3 of the components used and the absence of undesired reaction products during sintering or other processes [28]. This analysis is crucial for understanding the composition and stability of composites.

With increasing Gd_2O_3 supplementation, the intensity of Gd_2O_3 peaks was detected in XRD analysis, while a decrease in the intensity of the peaks corresponding to the Al and Sm_2O_3 phases was observed. Some Al and Sm_2O_3 peaks even disappeared completely. However, in 12Gd_2O_3 and 15Gd_2O_3 reinforced composites, the XRD peaks become more prominent and apparent. This can be attributed to the new morphology created in the matrix by the decreasing Al and Sm_2O_3 content as Gd_2O_3 reinforcement increases.

The XRD analysis results confirm that increasing Gd_2O_3 reinforcement becomes more prominent in the matrix. This is supported by the SEM-EDX analysis in Figures 4-6 and the relative densities in Figure 7. These results indicate that Gd_2O_3 reinforcement significantly changes the composite's phase distribution and morphology.
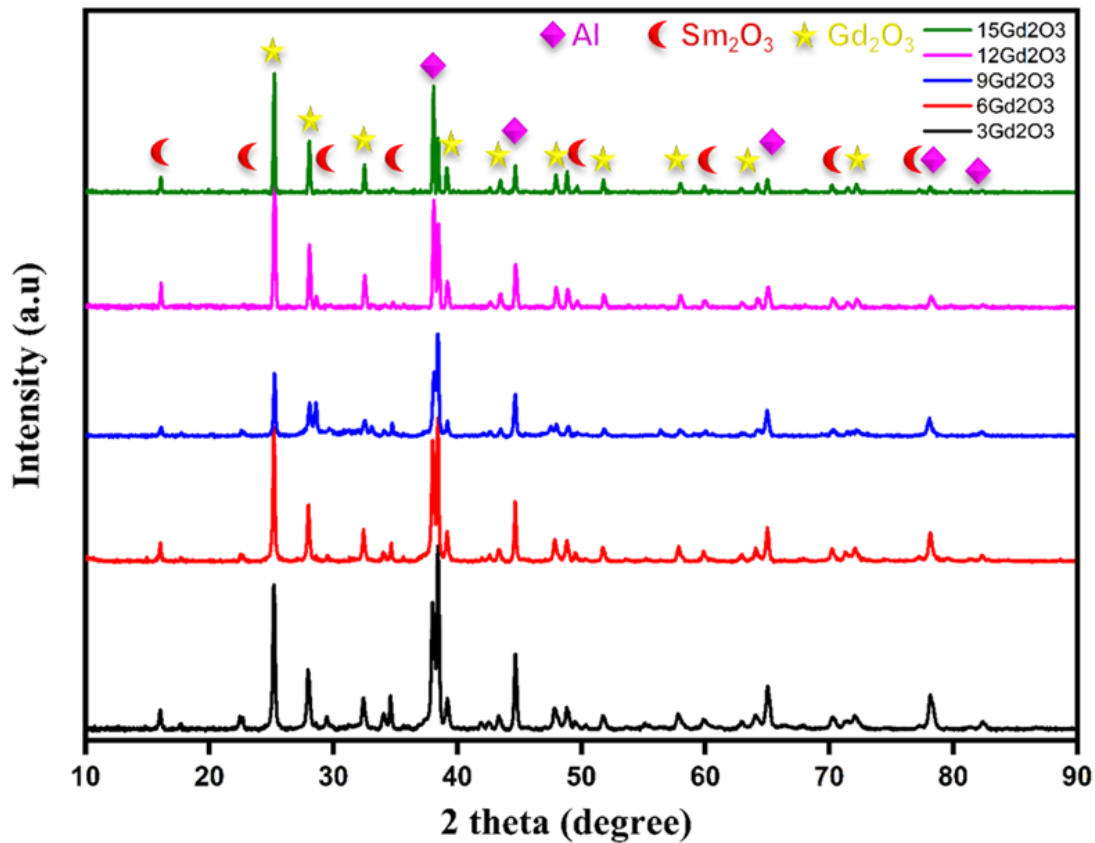
Fig. 3. X-ray diffraction patterns of Al-30Sm$_2$O$_3$-XGd$_2$O$_3$ (X = 3, 6, 9, 12, and 15) composites

3.2. SEM-EDX Analysis

A morphological investigation was carried out using SEM to evaluate the homogeneity and microstructural changes of the Al-Sm$_2$O$_3$-Gd$_2$O$_3$ composite powders produced at varying ratios by mechanical milling. SEM micrographs of the composites are presented in Figure 4. The micrographs on the left side show the general phase distribution at 500X (100 µm) magnification, while the micrographs on the right side provide a more detailed examination at 5000X (10 µm) magnification.

Gd$_2$O$_3$ reinforced at different ratios did not cause a noticeable change in morphology. In the general appearance, the gray irregular structures show Sm$_2$O$_3$, while the black matrix shows the structure dispersed as small particles together with Al and concentrated as the amount of Gd$_2$O$_3$ increases. This is evident from Figures 5 and 6. As can be seen from the relative densities, the void ratios in the composite changed as Gd$_2$O$_3$ increased; however, this difference was not at a level to change the morphology. The dark black regions represent the voids (Figure 4). As illustrated in Figures 4(c), 4(d), and 4(e), an increase in Gd$_2$O$_3$ reinforcement led to a partial reduction in relative density due to the rise in the number of voids. However, this resulted in a homogeneous distribution and improved the mechanical and physical properties of the composite. The gamma and thermal neutron attenuation properties increased, while the fast neutron attenuation ability decreased depending on the void ratio.

SEM-EDX analysis was performed on 3Gd$_2$O$_3$ and 15Gd$_2$O$_3$ composites; the results are presented in Figures 5 and 6. As seen in the SEM images, the mapping images show that Gd$_2$O$_3$ provides a homogeneous distribution. Moreover, EDX analysis confirmed that all of the powders that make up the composite were present. However, due to the low content and the fact that both reinforcing elements contain oxygen, it becomes difficult to analyze by Energy Dispersive X-ray Spectroscopy (EDX) [29].
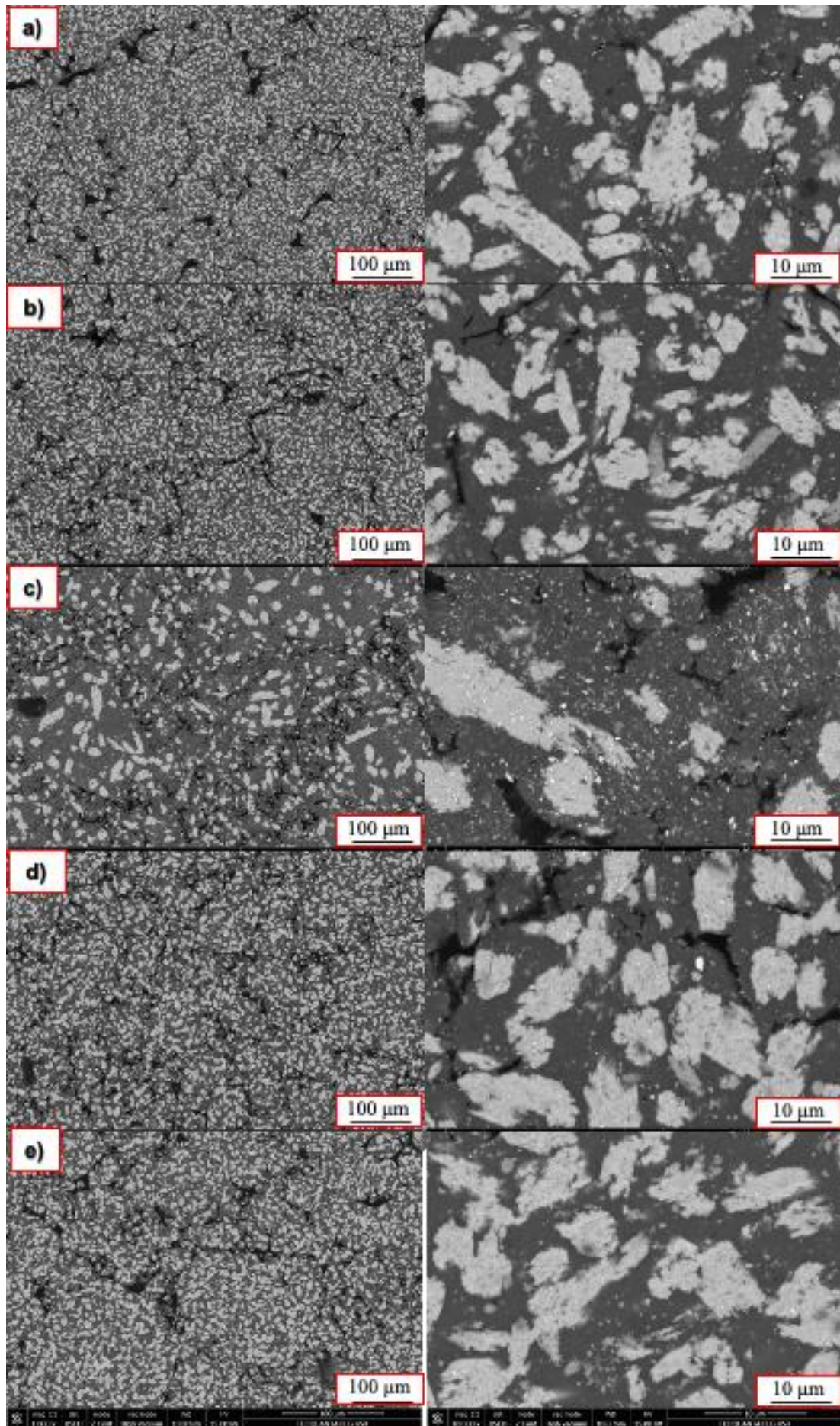
Figure 4. SEM image of a) 3Gd$_2$O$_3$, b) 6Gd$_2$O$_3$, c) 9Gd$_2$O$_3$, d) 12Gd$_2$O$_3$, and e) 15Gd$_2$O$_3$ composites
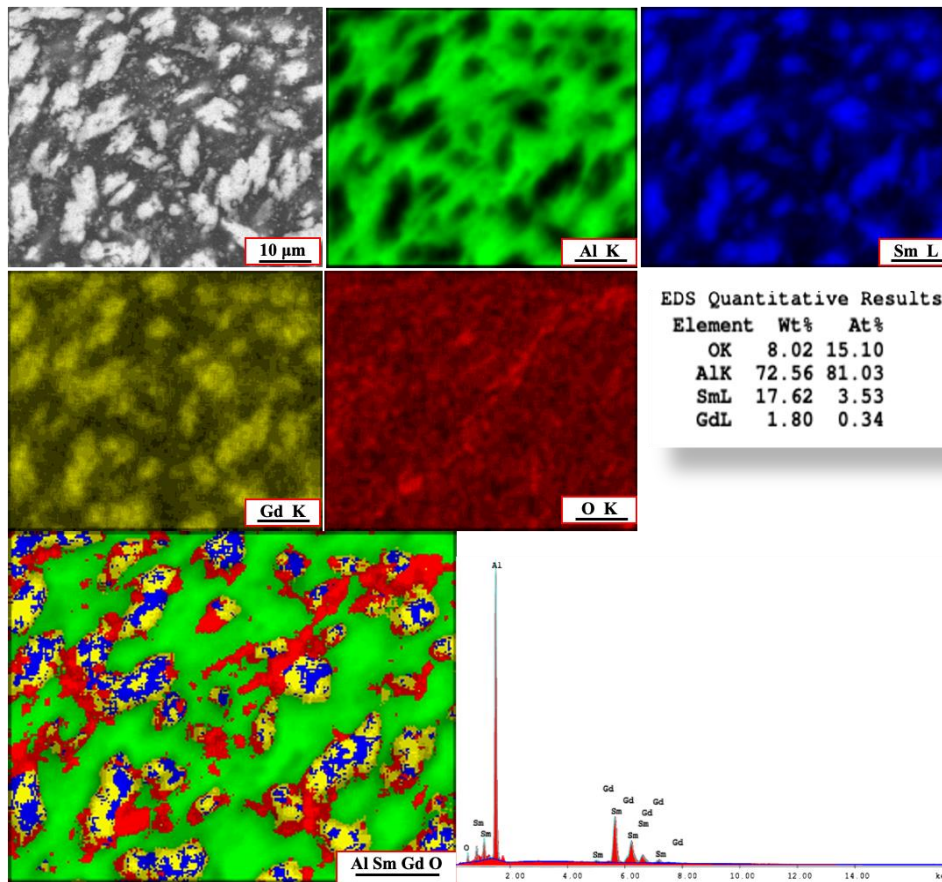
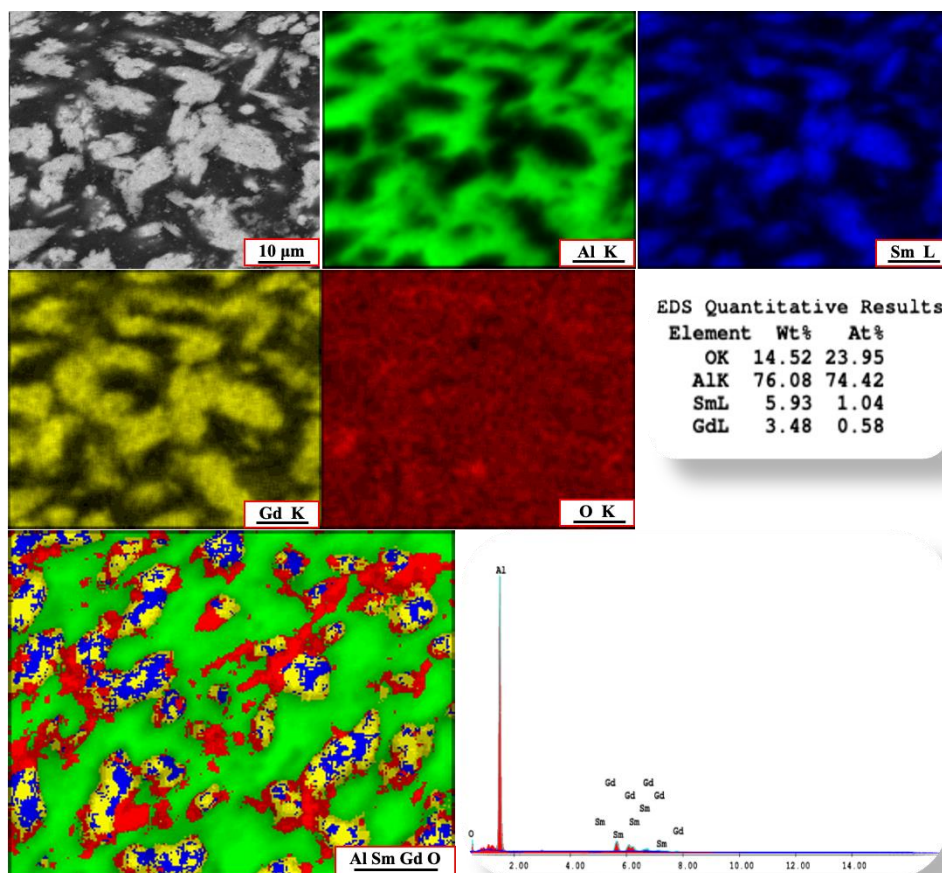**Figure 5.** SEM-EDX elemental mapping images of the 3Gd$_2$O$_3$ composite

Figure 6. SEM-EDX elemental mapping images of the 15Gd$_2$O$_3$ composite

3.3. Density and Microhardness Measurements

The Vickers hardness and relative density of Al-Sm_2O_3-Gd_2O_3 composites are illustrated in Figure 7. This research also investigated the mechanical properties of the Al-Sm_2O_3-Gd_2O_3 composites. The results show that the hardness values significantly increased with adding Gd_2O_3, from 137.2 HV with 3% Gd_2O_3 to 218.4 HV with 15% Gd_2O_3. This increase in hardness is directly attributed to the reduction of voids resulting from the homogeneous and compact microstructure facilitated by Gd_2O_3. These findings have practical implications for the potential use of these composites in applications that require high mechanical strength.

At a low reinforcement level of 3% Gd_2O_3, the composite exhibits a reduction in void ratio, contributing to the homogeneity of the microstructure. However, relative density values slightly decline with increasing Gd_2O_3 content, decreasing from 88.4% at 3% Gd_2O_3 to 86.1% at 15% Gd_2O_3. This suggests a relationship between the increase in hardness and density; however, microstructural arrangement and particle distribution alterations may play a more significant role.

Furthermore, the role of Gd_2O_3 reinforcement in optimizing void ratios and preventing particle aggregation is a crucial consideration. Lower Gd_2O_3 ratios may be more effective in achieving these benefits. However, as the Gd_2O_3 content increases, the standard deviation in hardness measurements suggests a decline in the material's microstructural properties. This decline negatively impacts the mechanical performance and structural consistency of the composite. Therefore, the Gd_2O_3 reinforcement ratio influences the mechanical, physical, neutron, and gamma absorption properties.
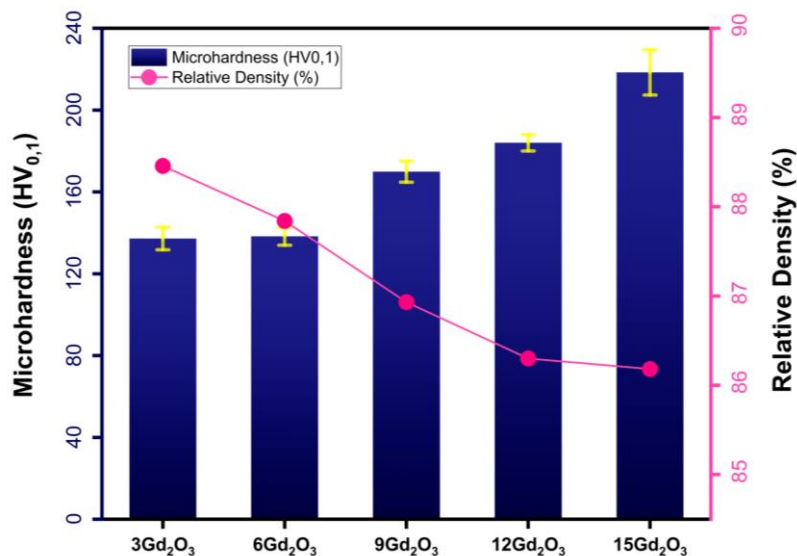
Figure 7. Comparison of microhardness and relative density of Al-30Sm_2O_3 composites reinforced with different amounts of Gd_2O_3

Figure 8 shows the wear rate and resistance values of Al-30Sm_2O_3 composites with different amounts of Gd_2O_3 reinforcement. The wear test results reveal that the 3Gd_2O_3 reinforced specimen exhibits a high wear rate and low wear resistance values. However, the 6Gd_2O_3 reinforced composite significantly increased compared to the 3Gd_2O_3 reinforced composite. Composites with 6Gd_2O_3 and 9Gd_2O_3 reinforcements showed almost similar values. However, 12Gd_2O_3 composite showed a significant increase while 15Gd_2O_3 composite showed an extreme rise. These findings underline the potential of Gd_2O_3 to increase wear resistance and reduce wear rate. For example, 15Gd_2O_3 supplementation showed the lowest wear and resistance rates. In practical terms, composites with higher Gd_2O_3 reinforcement can be used in applications where wear resistance is crucial. In conclusion, wear resistance and wear rate measurements show that with increasing Gd_2O_3 reinforcement, the wear rate decreases, and the wear resistance improves significantly. These findings revealed that Gd_2O_3 is a crucial reinforcing element in terms of mechanical properties by increasing wear resistance and decreasing wear rate even at low reinforcement ratios.
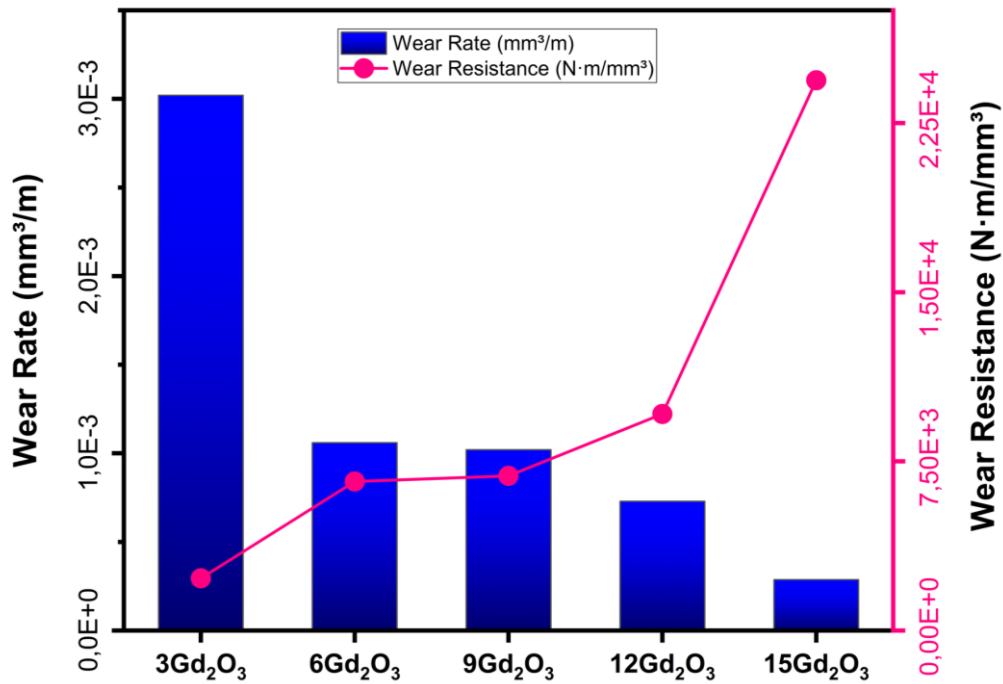
Figure 8. Wear rate and wear resistance of Al-30Sm$_2$O$_3$ composites reinforced with different amounts of Gd$_2$O$_3$

3.4. Electrochemical Corrosion Test

The polarization curves of the composites in 3.5 wt% NaCl solution at room temperature are shown in Figure 9(a). Potentiodynamic polarization curves were used to evaluate the behavior and the effect of varying Gd$_2$O$_3$ ratios on the corrosion properties. Figure 9 depicts these curves, and Table 3 presents the corresponding values. In addition, Figure 9b illustrates how Icorr values and corrosion rate are affected by varying the amount of Gd$_2$O$_3$ reinforcement. The corrosion current density (Icorr) and corrosion potential (Ecorr) values were determined by extrapolation of the cathodic polarization curves intersecting the Ecorr horizontal line. This result indicates that Gd$_2$O$_3$ reinforcement positively affects the corrosion resistance and creates a passive film effect.

The corrosion rate-reducing effect of Gd$_2$O$_3$ reinforcement has been present from the beginning despite the observed decrease in the relative density. For example, while the corrosion current density was 45.05 µA/cm² in the 3Gd$_2$O$_3$ composite, this value decreased to 0.175 µA/cm² in the 15Gd$_2$O$_3$ composite. Likewise, the corrosion rate decreased from 0.435 mm/year in the 3Gd$_2$O$_3$ composite to 0.0016 mm/year in the 15Gd$_2$O$_3$ composite. This continuous decrease indicates that Gd$_2$O$_3$ slows corrosion by forming a passive film on the aluminum matrix, a behavior that is crucial for understanding the material's corrosion resistance.

Although the relative density of 15Gd$_2$O$_3$ composites exhibits a low value of (86.1%), this decrease in corrosion rate continues due to the passive film effect created by the Gd$_2$O$_3$ reinforcement. This indicates that Gd$_2$O$_3$ improves the material's performance by suppressing micro-galvanic effects and forming a more corrosion-resistant layer [30]. In conclusion, these findings underscore the critical role of the Gd$_2$O$_3$ reinforcement ratio in determining the mechanical properties, thermal neutron and gamma attenuation properties, and corrosion resistance of Al-Sm$_2$O$_3$ composites. Moreover, the corrosion rate decreases continuously with increasing Gd$_2$O$_3$ reinforcement, and the passive film-forming effect of Gd$_2$O$_3$ increases the corrosion resistance despite the decrease in relative density. This reveals that careful selection of optimum Gd$_2$O$_3$ ratios is critical in improving the corrosion properties of composites.
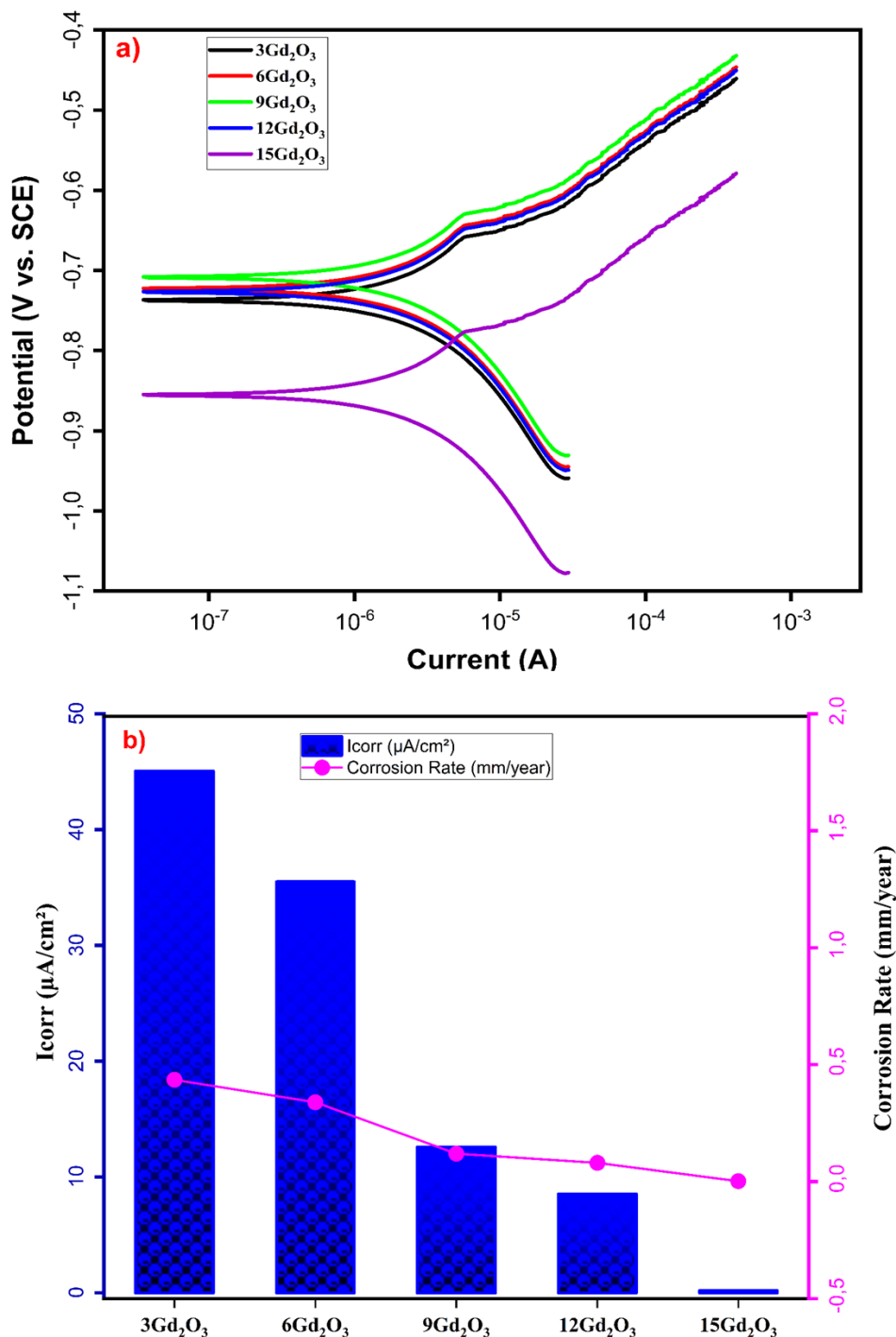
Figure 9. a) Polarization curves b) the variation trend of I_{corr} and the change of corrosion rate of Al-Sm$_2$O$_3$-Gd$_2$O$_3$ composites

Table 3. Polarization results of the Al-Sm$_2$O$_3$-Gd$_2$O$_3$ composites

Materials	Ecorr (mV)	Icorr (µA/cm²)	Corrosion Rate (mm/year)
3Gd$_2$O$_3$	-737	45,052	0,435
6Gd$_2$O$_3$	-708	35,473	0,339
9Gd$_2$O$_3$	-705	12,578	0,119
12Gd$_2$O$_3$	-770	8,526	0,080
15Gd$_2$O$_3$	-887	0,175	0,001

3.5 Neutron and Gamma Radiation Shielding Properties

The Monte Carlo simulation program MCNP was used to create a radiation shielding model of Al-Sm_2O_3-Gd_2O_3 composites. MCNP is a versatile software package for computing neutron, photon, and electron transport problems in complex three-dimensional geometric structures. Figure 10 depicts the thermal neutron macroscopic cross-section and attenuation rate of 0.02 cm thick Al-Sm_2O_3-Gd_2O_3 composites. These composites' thermal neutron macroscopic cross-section values were 32.3 cm^{-1}, 47.0 cm^{-1}, 61.8 cm^{-1}, 77.0 cm^{-1}, and 93.7 cm^{-1}, respectively. This thermal neutron macroscopic cross-section reduction directly affected the composite's neutron attenuation rate. The corresponding neutron attenuation rates for different Gd_2O_3 reinforcement levels were 47.6% for 3% Gd_2O_3, 60.9% for 6% Gd_2O_3, 70.9% for 9% Gd_2O_3, 78.5% for 12% Gd_2O_3, and 84.5% for 15% Gd_2O_3.

The data indicate a significant improvement in the neutron attenuation performance of the composites as Gd_2O_3 content increases. While a lower neutron attenuation rate is observed with 3% Gd_2O_3 reinforcement, levels as high as 84.5% are achieved with 15% Gd_2O_3. This indicates that Gd has a high neutron absorption capacity, and increasing Gd_2O_3 content significantly increases the neutron attenuation rate. The Gd-157 isotope has the highest thermal-neutron capture cross-section of any stable nuclide: about 259,000 bar. Only xenon-135 has a higher capture cross-section, about 2.0 million bar, but this isotope is radioactive. In conclusion, these findings demonstrate that Gd_2O_3 reinforcement plays a vital role in improving the neutron attenuation properties of composites and highlights its potential for advanced industrial applications. These implications inspire us to explore the possibility of Gd_2O_3 in materials science and engineering, motivating us to push the boundaries of our understanding and application of these materials.
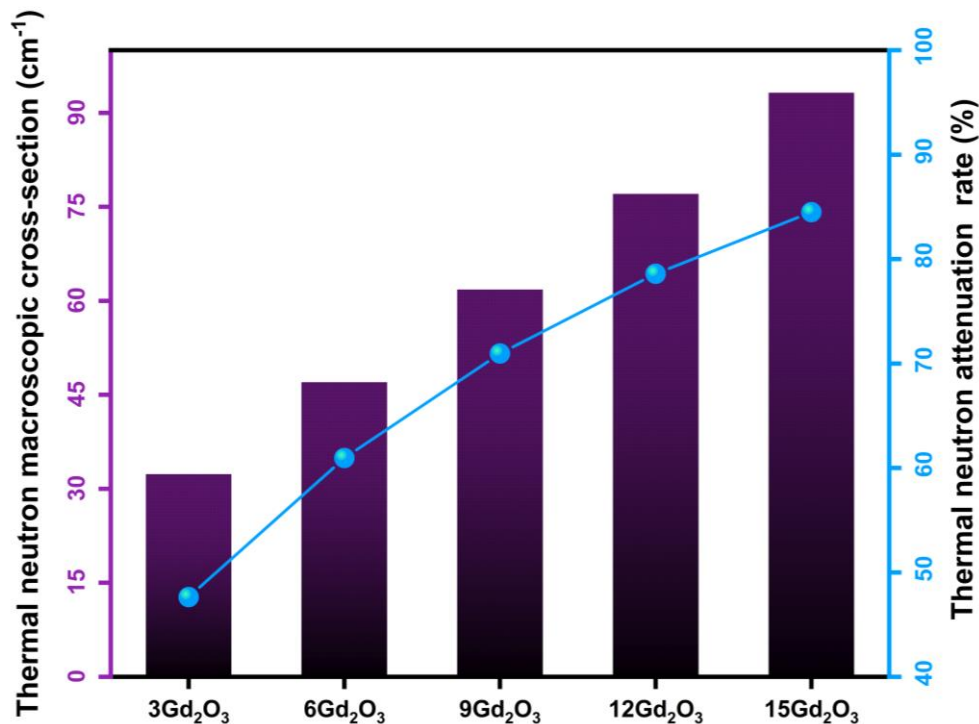
Figure 10. Thermal neutron macroscopic cross-section and attenuation rate graph of Al-Sm_2O_3-Gd_2O_3 composites

Figure 11 illustrates the fast neutron macroscopic cross-section and attenuation ratios for Al-Sm_2O_3-Gd_2O_3 composites based on 2 cm thickness. In the graph, with increasing Gd_2O_3 reinforcement, fast neutron attenuation rates decrease in parallel with the fast neutron macroscopic cross-section. For example, while the cross section was measured as 0.178 cm^{-1} with 3% Gd_2O_3 reinforcing, this value decreased to 0.175 cm^{-1} with 15% Gd_2O_3 reinforcing. These data show a significant decrease in the fast neutron cross-section area as Gd_2O_3 reinforcing increases. The fast neutron attenuation rates, which change in proportion to these values, decreased

from 30.0% with 3% Gd_2O_3 to 29.5% with 15% Gd_2O_3. In this context, it can be inferred that the increase in Gd_2O_3 content generally leads to a decrease in the fast neutron cross-section and attenuation ratio. An increase in Gd_2O_3 content generally led to a reduction in the fast neutron cross-section and attenuation rate. The decrease in the fast neutron macroscopic cross-section and attenuation rate with increasing Gd_2O_3 reinforcement can be explained by the fact that the propagation of neutrons in a material is inversely proportional to the relative density of the material. A hollow structure with a low relative density allows neutrons to propagate through the material along longer accessible paths [31]. This is because the interatomic distance increases in materials with low relative density, and the probability of neutrons interacting with atomic nuclei decreases. Consequently, a decrease in relative density within the same material is predicted to result in fewer neutrons interacting with the material, increasing neutron permeability. However, this phenomenon depends on neutron energy and the material's atomic structure.
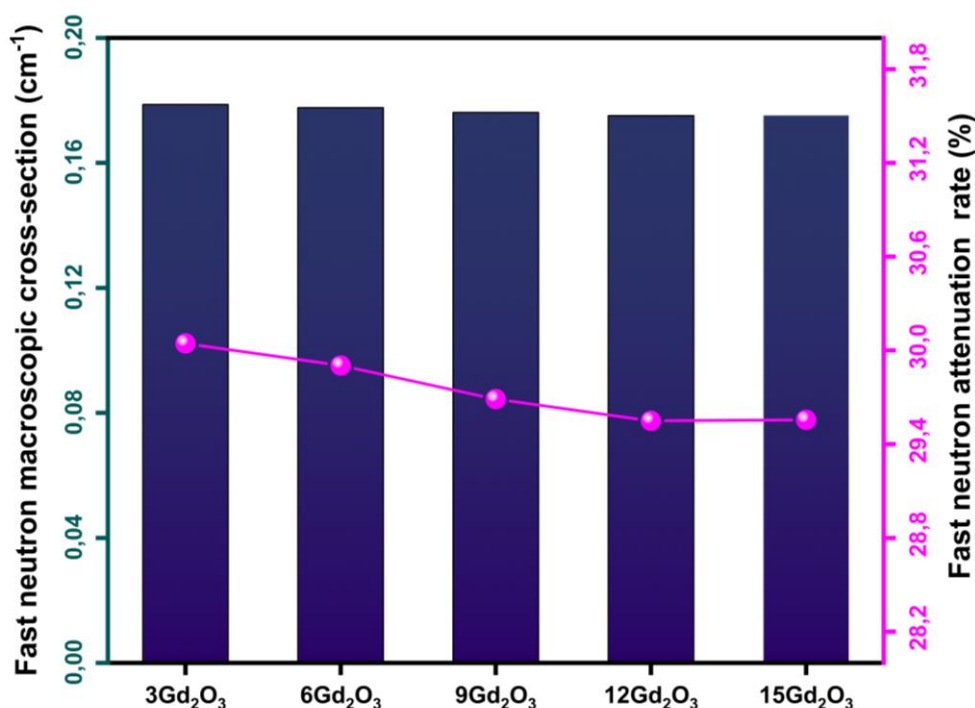
Figure 11. Fast neutron macroscopic cross-section and attenuation rate graph of Al-Sm_2O_3-Gd_2O_3 composites

The linear attenuation coefficient (LAC), which the Beer-Lambert Law can calculate, is an essential indicator for highlighting the radiation shielding properties of a material. Figure 12 presents the LAC and photon attenuation ratio of Al-Sm_2O_3-Gd_2O_3 composites at 0.478 MeV photon energy. The LAC value for the 3% Gd_2O_3 reinforced composite was calculated as 0.28 cm^{-1}. A significant increase in LAC was observed with the rise of Gd_2O_3 supplementation, and a value of 0.30 cm^{-1} was obtained for 15% Gd_2O_3. Regarding photon attenuation, the composite containing 3% Gd_2O_3 exhibited an attenuation rate of 43.7%, which increased to 45.9% with 15% Gd_2O_3 reinforcement. This shows that Gd_2O_3 reinforcement significantly enhances the photon attenuation properties of composites. Such improvements are critical for various fields, such as home appliances, smart device displays, telecommunications, military purposes, and medical devices that require enhanced radiation shielding properties. These findings have revealed the benefits of Gd_2O_3 in photon interactions and its role as a critical reinforcing element to increase the LAC values of Al-$30Sm_2O_3$.

Additionally, to validate the established geometry, gamma-ray attenuation results obtained from the MCNP simulations were compared with the XCOM database, confirming the model's accuracy. The Half Value Layer (HVL) and Mean Free Path (MFP) (where μ is the linear attenuation coefficient) values were calculated using the following formulas to evaluate the shielding performance of the materials. These results, along with their significance, are presented in Table 4. The obtained results are consistent with the literature [19].

$$\text{HVL} = \frac{ln_2}{\mu}$$
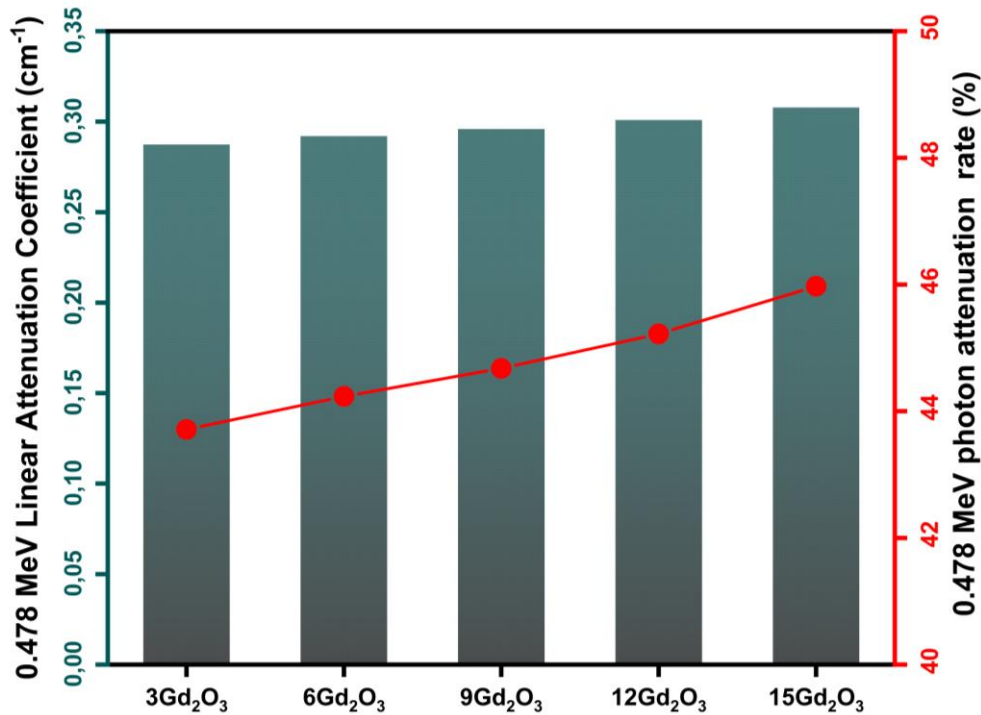
$$\text{MFP} = \frac{1}{\mu}$$

Figure 12. Gamma-ray linear attenuation coefficient and attenuation rate of Al-Sm$_2$O$_3$-Gd$_2$O$_3$ composites

Table 4. Calculated Half Value Layer (HVL), Mean Free Path (MFP), and Mass Attenuation Coefficient (MAC) results of the Al-Sm$_2$O$_3$-Gd$_2$O$_3$ composites

Materials	MAC (cm^2/g)	HVL (cm)	MFP (cm)
3Gd$_2$O$_3$	0,0943	2,412	3,480
6Gd$_2$O$_3$	0,094	2,373	3,424
9Gd$_2$O$_3$	0,095	2,341	3,378
12Gd$_2$O$_3$	0,096	2,303	3,322
15Gd$_2$O$_3$	0,0968	2,251	3,248

4. Conclusion

In this study, Al-30Sm$_2$O$_3$-XGd$_2$O$_3$ (X=3, 6, 9, 12, and 15) composites were designed and successfully fabricated for the first time. The effects of Gd$_2$O$_3$ reinforcement on the composites' mechanical and attenuation properties of gamma and neutron radiation were investigated. Thermal neutron, fast neutron, and gamma attenuation performances were analyzed by MCNP6.2 code, while mechanical and physical properties were evaluated by wear, hardness, density, and corrosion tests. X-ray diffraction (XRD) analysis revealed various peaks corresponding to Al-Sm$_2$O$_3$-Gd$_2$O$_3$ composites, and it was determined that no intermetallic phase or compound was formed due to grinding and sintering processes. (SEM-EDX) analyses studied the morphology of the composites, and a partial increase in void ratio was observed with Gd$_2$O$_3$ reinforcement.

The composites' density, hardness, and wear resistance increased significantly with increasing Gd_2O_3 reinforcement, but a partial decrease in the relative density occurred. Hardness and wear resistance reached the highest levels with 15% Gd_2O_3 reinforcement. At the same time, Gd_2O_3 reinforcement reduced the corrosion rate, but a significant increase in corrosion rate was observed in the composite containing 15% Gd_2O_3. The rise in Gd_2O_3 reinforcement results in a noticeable increase in the hardness of the composite, rising from 137.2 HV to 218.4 for 15 Gd_2O_3.

In addition, MCNP6.2 simulations showed that Gd_2O_3 reinforcement increased the thermal macroscopic neutron cross-section and the LAC of gamma rays. However, a decrease in the macroscopic cross-section of fast neutrons was recorded. The reduction in the relative density increased the void ratio of the composites, facilitating the passage of fast neutrons. These results reveal that Gd_2O_3 reinforcement significantly affects the composites' physical properties and radiation attenuation performances. MCNP6.2 simulations confirmed that Gd_2O_3 reinforcement improved the neutron and gamma shielding properties, increasing the thermal macroscopic neutron cross-section and gamma-ray LAC while decreasing the fast neutron macroscopic cross-section.

For future studies, it is suggested that the amount of reinforcement be optimized as well as parameters such as grinding time and sintering temperature, taking into account the improvements of Gd_2O_3 reinforcement on radiation shielding and mechanical properties. Furthermore, adding different reinforcements such as B_4C, Sm, Eu, Cd, B, Gd, Sm_2O_3, and Al_2O_3 would be helpful for a more comprehensive investigation of the mechanical and radiation shielding properties.

Author Contributions

The author read and approved the final version of the paper.

Conflict of Interest

The author declares no conflict of interest.

Ethical Review and Approval

No approval from the Board of Ethics is required.

References

[1] M. Lalkovicova, *Neuroprotective agents effective against radiation damage of central nervous system*, Neural Regeneration Research 17 (2022) 1885–1892.

[2] G.A. Thomas, P. Symonds, *Radiation Exposure and Health Effects - is it Time to Reassess the Real Consequences?*. Clinical Oncology, (2016) 28(4), 231–236.

[3] Y. Gaylan, B. Avar, *Al–B4C-(Gd, Gd2O3) composite materials: Synthesis and characterization for neutron shielding applications*, Nuclear Engineering and Technology (2024).

[4] N. Ekinci, N.A.M. Alsaif, Z.Y. Khattari, Y.S. Rammah, B. Aygün, Y. Kurucu, S. Sarıtaş, *Evaluation of lithium tetra borate glass-ceramics: Structural, physical and radiation safety properties using experimental and theoretical methods*, Nuclear Engineering and Technology (2024).

[5] B. Aygun, I. Bilici, C.U. Deniz, B. Oz, M.I. Sayyed, A. Karabulut, *Development of novel composite materials containing rice bran wax and waste polyethylene for neutron shielding applications*, Progress in Nuclear Energy 174 (2024) 105262.

[6]   C. Kursun, M. Gao, S. Guclu, Y. Gaylan, K.A. Parrey, A.O. Yalcin, *Measurement on the neutron and gamma radiation shielding performance of boron-doped titanium alloy Ti 50 Cu 30 Zr 15 B 5 via arc melting technique*, Heliyon 9 (2023) 2405–8440.

[7]   H.S. Chen, W.X. Wang, Y.L. Li, P. Zhang, H.H. Nie, Q.C. Wu, M. Carlo, *The design, microstructure and tensile properties of B4C particulate reinforced 6061Al neutron absorber composites*, Journal of Alloys and Compounds 632 (2015) 23–29.

[8]   K. Deng, J. Shi, C. Wang, X. Wang, Y. Wu, K. Nie, K. Wu, *Composites: Part A Microstructure and strengthening mechanism of bimodal size particle reinforced magnesium matrix composite*, Composites Part A 43 (2012) 1280–1284.

[9]   G. Luo, J. Wu, S. Xiong, Q. Shen, C. Wu, *Microstructure and mechanical behavior of AA2024 / B 4 C composites with a network reinforcement architecture*, Journal of Alloys and Compounds 701 (2017) 554–561.

[10] I. Topcu, H. O. Gulsoy, N. Kadioglu, A. N. Gulluoglu, *Processing and mechanical properties of B4C reinforced Al matrix composites*, Journal of Alloys and Compounds 482 (2009) 516–521.

[11] P. Zhang, Y. Li, W. Wang, Z. Gao, B. Wang, *The design, fabrication and properties of B4C/Al neutron absorbers*, Journal of Nuclear Materials 437 (2013) 350–358.

[12] Y. Gaylan, B. Avar, M. Panigrahi, B. Aygün, A. Karabulut, *Effect of the B4C content on microstructure, microhardness, corrosion, and neutron shielding properties of Al–B4C composites*, Ceramics International 49 (2023) 5479–5488.

[13] Y. He, H. Xu, Y. Liu, Y. Chen, Z. Ji, *Strengthening mechanism of B4C@APC/Al matrix composites reinforced with bimodal-sized particles prepared by hydrothermal carbonized deposition on chips*, Journal of Materials Science & Technology 123 (2022) 60–69.

[14] R. G. Abrefah, R. B. M. Sogbadji, E. Ampomah-Amoako, S. A. Birikorang, H. C. Odoi, B. J. B. Nyarko, *Comparison of the effects of cadmium-shielded and boron carbide-shielded irradiation channel of the Ghana Research Reactor-1*, Nuclear Engineering and Design 241 (2011) 3017–3020.

[15] S. Wan, W. Wang, H. Chen, J. Zhou, Y. Zhang, R. Liu, R. Feng, *155/157Gd areal density: A model for design and fabrication of Gd2O3/316L novel neutron shielding composites*, Vacuum 176 (2020).

[16] R. Florez, H. A. Colorado, C. H. C. Giraldo, A. Alajo, *Preparation and characterization of Portland cement pastes with Sm2O3 microparticle additions for neutron shielding applications*, Construction and Building Materials 191 (2018) 498–506.

[17] C. Kursun, M. Gao, A. O. Yalcin, K. A. Parrey, Y. Gaylan, *Structure, mechanical, and neutron radiation shielding characteristics of mechanically milled nanostructured (100-x)Al-xGd2O3 metal composites*, Ceramics International (2024).

[18] D.-Y. Zhang, X.-Y. Shen, Q. Ruan, X.-L. Xu, S.-P. Yang, Y. Lu, H.-Y. Xu, F.-L. Hao, *Effects of subchronic samarium exposure on the histopathological structure and apoptosis regulation in mouse testis*, Environ Toxicol Pharmacol 37 (2014) 505–512.

[19] Y. Gaylan, I. E. Dag, S. Caglar, B. Avar, *Investigation of mechanical and radiation shielding properties of Sm–Sm2O3 reinforced Al–B4C composite*, Radiation Physics and Chemistry 226 (2025) 112325.

[20] H. Guo, Z. Zhang, Y. Zhang, Y. Cui, L. Sun, D. Chen, *Improving the mechanical properties of B4C/Al composites by solid-state interfacial reaction*, Journal of Alloys and Compounds 829 (2020) 154521.

[21] Q. Lin, P. Shen, F. Qiu, D. Zhang, Q. Jiang, *Wetting of polycrystalline B4C by molten Al at 1173–1473K*, Scripta Materialia 60 (2009) 960–963.

[22] R.-F. Guo, S.-M. Chen, P. Shen, *Influence of Si, Ti, and Cu as alloying elements on the wettability and reactivity of an Al/B4C system*, Journal of Materials Research and Technology 27 (2023) 6104–6116.

[23] L. T. Jiang, Z. G. Xu, Y. K. Fei, Q. Zhang, J. Qiao, G. H. Wu, *The design of novel neutron shielding (Gd+B4C)/6061Al composites and its properties after hot rolling*, Composites Part B: Engineering 168 (2019) 183–194.

[24] P. Zhang, C. Jia, J. Li, W. Wang, *Shielding composites for neutron and gamma-radiation with Gd2O3@W core-shell structured particles*, Materials Letters 276 (2020) 128082.

[25] S. Niksarlıoğlu, F. Akman, M.E. Pekdemir, S. Yalçın Kuzu, M.R. Kaçal, M. Yılmaz, *An extensive investigation on gamma shielding properties of PLA/Gd2O3 nanocomposites*, Radiation Physics and Chemistry 208 (2023) 110936.

[26] S. Cong, Y. Li, G. Ran, W. Zhou, Q. Feng, *Microstructure and its effect on mechanical and thermal properties of Al-based Gd2O3 MMCs used as shielding materials in spent fuel storage*, Ceramics International 46 (2020) 12986–12995.

[27] M. C. Team, MCNP-A general Monte Carlo N-particle transport code, Version 5 Volume I: Overview and Theory X-5 Monte Carlo Team, 2003.

[28] H. Ozdogan, O. Kilicoglu, F. Akman, O. Agar, *Comparison of Monte Carlo simulations and theoretical calculations of nuclear shielding characteristics of various borate glasses including Bi, V, Fe, and Cd*, Applied Radiation and Isotopes 189 (2022) 110454.

[29] S. Caglar, M. F. Kilicaslan, A. Atasoy, H. Tiryaki, M. Erkovan, S. jik Hong, *Effect of heat treatment on magnetic properties of nanocomposite Nd-lean Nd7Fe73B20 ribbons*, Journal of Materials Science: Materials in Electronics 32 (2021) 2338–2345.

[30] Y. Zhu, T. Zhao, X. Yu, Y. Zhu, Q. Shen, R. Li, G. Xie, *Effect of gadolinium trioxide on anode performance of aluminum-air batteries*, Ionics 29 (2023) 4723–4731.

[31] H. Akyıldırım, *Calculation of fast neutron shielding parameters for some essential carbohydrates*, Erzincan University Journal of Science and Technology 12 (2019) 1141–1148.